Journal of Hazardous Materials 186 (2011) 984–990

Contents lists available at ScienceDirect

Journal of Hazardous Materials

journal homepage: www.elsevier.com/locate/jhazmat

Microwave-enhanced synthesis of magnetic porous covalent triazine-based framework composites for fast separation of organic dye from aqueous solution

Wang Zhang[a], Fei Liang[a], Cun Li[a], Ling-Guang Qiu[a,*], Yu-Peng Yuan[a], Fu-Min Peng[a], Xia Jiang[a], An-Jian Xie[a], Yu-Hua Shen[a], Jun-Fa Zhu[b]

[a] Laboratory of Advanced Porous Materials, School of Chemistry and Chemical Engineering, Anhui University, 3rd Feixi Road, Hefei 230039, Anhui Province, China
[b] National Synchrocyclotron Radiation Laboratory, University of Science and Technology of China, Hefei 230029, China

ARTICLE INFO

Article history:
Received 26 September 2010
Received in revised form
22 November 2010
Accepted 23 November 2010
Available online 27 November 2010

Keywords:
Covalent triazine-based framework
Porous material
Microwave-assisted synthesis
Magnetic separation
Dye

ABSTRACT

A novel type of magnetic porous carbonaceous polymeric material, CTF/Fe_2O_3 composite (CTF = covalent triazine-based framework), has been synthesized by a facile microwave-enhanced high-temperature ionothermal method. By selecting $ZnCl_2$ as a reaction medium and the Lewis acid catalyst, and choosing $FeCl_3{\cdot}6H_2O$ as an iron oxide precursor, a series of CTF/Fe_2O_3 composites with different γ-Fe_2O_3 contents has been prepared in 60 min. The resulting samples were characterized by the X-ray diffraction (XRD), X-ray photoelectron spectroscopy (XPS), scanning electron microscopy (SEM), transmission electron microscopy (TEM), vibration sample magnetometer (VSM), and N_2 sorption–desorption isotherms. The obtained CTF/Fe_2O_3 composites exhibit high surface areas (930–1149 $m^2\,g^{-1}$), and their saturation magnetizations at 300 K vary from 1.1 to 5.9 emu g^{-1}, depending respectively on different Fe_2O_3 contents (6.43–12.43 wt%) in the CTF/Fe_2O_3 composites. The CTF/Fe_2O_3 composites were applied to remove organic dye from aqueous solution by selecting methyl orange as a model molecule, and both high adsorption capacity (291 mg g^{-1}, corresponding to 0.889 mmol g^{-1}) and fast adsorption kinetics (k_{ads} = 4.31 $m^2\,mg^{-1}\,min^{-1}$) were observed.

1. Introduction

Dyes are becoming major sources of environmental pollution, because discharging of dyes into water resources can significantly affect the aquatic life and food web [1]. Furthermore, owing to their complex aromatic structures, almost all synthetic dyes are difficult to be biodegraded, and thus are recognized as difficult-to-treat pollutants [2]. Adsorption technique is quite popular due to simplicity and high efficiency. Various adsorbents have been developed and applied to remove dyes from polluted water [3], among them porous materials such as activated carbons offer an attractive and inexpensive option for efficient removal of various organic contaminants from water due to their high surface areas [4,5]. Although commercial activated carbon is a preferred adsorbent for dye removal, it is difficult to separate the absorbents from aqueous solution, thus limiting its applications in many fields [3,6].

The application of magnetic particle technology to solve environmental problems has received considerable attention in recent years. By the application of an external magnetic field, the adsorbents can easily be separated from the solution. Many kinds of magnetic adsorbents, such as magnetic nanoparticles [7,8], organic group-modified [9] and polyelectrolyte-bound iron oxide magnetic nanoparticles [10], activated carbon/iron oxide magnetic composites [11–13], activated carbon/$CoFe_2O_4$ composites [14], magnetic multi-walled carbon nanotubes (MWCNTs) filled with Fe_2O_3 particles [15], have been developed, and their adsorption properties for the removal of dyes from aqueous solutions were investigated. However, the synthesis procedures of these magnetic materials are commonly complicated and require several steps. Moreover, many of these materials have low surface areas, thus exhibiting small adsorption capacities (usually lower than 0.30 mmol g^{-1}) and limiting their practical applications.

Covalent triazine-based frameworks (CTFs) are a new kind of high-performance carbonaceous polymeric material developed very recently [16]. Compared with many other porous organic materials formed from highly expensive organic monomers and crosslinkers such as phenyl polyboronic acids and polyhydroxy aromatic compounds [17–19], CTFs are prepared from cheap aromatic nitriles through a simple ionothermal polymerization reaction. These nanoporous organic materials possess remarkably high surface areas. Most importantly, this novel kind of robust porous organic networks exhibits extremely high thermal (up to 500 °C) and chemical stability [20–24]. This makes these porous materials great potential in industrial applications. Interestingly, these carbonaceous polymers were found to behave as an exceptional adsorbent toward large organic molecules such as organic dyes;

* Corresponding author. Tel.: +86 551 5108212; fax: +86 551 5108212.
E-mail addresses: lgqiu@ahu.edu.cn, lgahu@163.com (L.-G. Qiu).

0304-3894/$ – see front matter © 2010 Elsevier B.V. All rights reserved.
doi:10.1016/j.jhazmat.2010.11.093

their adsorption capacity for Yellow 3G-P can reach 1300 mg g^{-1}, which is several times larger than that of activated carbon for dye adsorption [25].

In our recent work, we developed a novel microwave-enhanced high-temperature ionothermal method for highly efficient synthesis of these porous carbonaceous polymers [26]. CTF samples with high surface areas could easily be obtained in tens of minutes by using such the microwave-enhanced ionothermal method, while polymerization of aromatic nitriles under conventional ionothermal conditions has to be carried out at high temperatures (400–700 °C) for a long reaction time (20–116 h). Based on such the microwave-enhanced ionothermal method, in the present work, we hope to illustrate a simple yet highly efficient approach to magnetic CTF composites by introducing $FeCl_3{\cdot}6H_2O$ into the reaction medium. A series of CTF/Fe_2O_3 composites with different γ-Fe_2O_3 contents was obtained in 60 min (Fig. 1). The as-synthesized materials possess both high surface areas and magnetic characteristics for their potential applications in magnetic separation. Their adsorption properties were preliminarily demonstrated by adsorbing methyl orange (MO). The results suggest that these magnetic CTF-based composites exhibit an excellent adsorption capacity (291 mg g^{-1}, corresponding to 0.889 mmol g^{-1}) and a rapid adsorption kinetics (k_{ads} = 4.31 m^2 mg^{-1} min^{-1}), as well as a perfect magnetic separation performance, for the removal of MO from aqueous solution. To the best of our knowledge, this is the first example of the synthesis of magnetic CTF-based composite and its application in magnetic separation.

2. Experimental

2.1. Preparation of materials

Anhydrous Zinc chloride was purchased from Sinopharm (Shanghai) Chemical Reagent Co., Ltd., and 1,4-dicyanobenzene (DCB) was purchased from Aldrich. Other chemical reagents and organic solvents were commercially purchased and used as received.

In a typical synthesis, a desired amount of ferric chloride hexahydrate ($FeCl_3{\cdot}6H_2O$) depending on different synthesis conditions was dissolved in 0.5–1.5 mL of ethanol, and 1,4-dicyanobenzene (2.0 g, 15.6 mmol) was then added. After mixing anhydrous zinc chloride ($ZnCl_2$, 10.6 g, 77.9 mmol) with the mixture of DCB and $FeCl_3{\cdot}6H_2O$, the composite was transferred into a 25 mL crucible. The crucible was then put in a microwave oven (Glanz P70D20SP-DF, Shenzhen, China). Although the preparation of CTFs has to be carried out in a sealed quart ampoule under vacuum using the conventional high-temperature ionothermal method, CTF-based magnetic composites could easily be obtained by microwave high-temperature ionothermal method at atmospheric pressure in the present work. The reaction temperatures were determined to be 500–550 °C at different reaction times by using an infrared thermometer. After microwave irradiation for 1 h at a microwave power output of 350 W, the reaction mixture was allowed to cool to room temperature. The resulting solid was washed with a large amount of diluted hydrochloride acid solution (0.1 mol L^{-1}) to remove the residual zinc salts. Finally, the sample was filtered off, washed with water and tetrahydrofuran, and then dried at 150 °C in vacuum (0.01 MPa).

CAUTION: High temperature of the crucible during and after the reaction may lead to the crack of the microwave oven salver. So thermal isolation between crucibles and the microwave oven salver should be guaranteed.

2.2. Characterization

Powder X-ray diffraction (XRD) data were recorded using a step scan model with a range of 5–60° 2θ on a Philips-1700X diffractometer (Cu-Kα radiation, λ = 0.154178 nm). X-ray photoelectron spectroscopy (XPS) was obtained using a Thermo-VG ESCALAB 250. FT-IR spectra (KBr pellets) were recorded in the 400–4000 cm^{-1} range using a Nocolet Nexus 870 FT-IR spectrometer. Transmission electron microscope (TEM) studies were carried out on a JEOL JSM-2100 electron microscope operating at 200 kV, and scanning electron microscope (SEM) images were obtained at 5 kV from a Hitachi S4800 scanning electron microscope. Nitrogen sorption–desorption isotherms were measured at 77 K using a Micromeritics 2020M + C system after the samples were degassed at 150 °C overnight, and surface areas of the samples were determined by the BET method. Elemental analysis of C, H and N was carried out on a Vario ELIII. To determine Fe and Zn contents of the composites, the sample (5 mg) was added into a 25 mL crucible, and heated to 600 °C in a muffle furnace for 5 h. The residue was then dissolved in 10 mL condensed nitric acid and transferred into 100 mL volumetric flask and diluted with deionized water. And then Fe and Zn contents in each solution were determined by atomic absorption spectrometry (AAS) using a Thermo Elemental, USA M6 spectrometer. The magnetization curves were measured at 300 K under a varying magnetic field from −10 to 10 kOe on a BHV-55 vibration sample magnetometer (VSM).

2.3. Adsorption of methyl orange

Dye adsorption experiment was performed by choosing MO as a model molecule. After adding 25 mg of CTF/Fe_2O_3 composite to 50 mL of 50 mg L^{-1} MO aqueous solution, the conical flask containing the mixture solution was fixed on a shaker at 25 °C. The decaying trend of MO concentration versus contact times was followed by UV–vis spectroscopy (Shimadzu UV-1800) at 464 nm at various times. To determine the adsorption isotherms at 25 °C, 2 mg CTF/Fe_2O_3 composite was added to a series of MO solutions (30 mL) with various initial concentrations (5 – 50 mg L^{-1}), respectively, the conical flasks containing the mixture solution were shaken on a shaker at 25 °C for 15 h. The amounts of dyes adsorbed at different contact times were calculated from Eq. (1) [11,14]:

$$q_t = \frac{(c_0 - c_t)V}{mS_{BET}} \quad (1)$$

where q_t (mg m^{-2}) is the amount of dye adsorbed per square meter of adsorbent at time t, c_0 (mg L^{-1}) is the initial concentration of dye in the solution, and c_t (mg L^{-1}) is the concentration of dye at time t. V (L) is the volume of the solution, m (g) is the mass of the adsorbent used, and S_{BET} (m^2 g^{-1}) is the BET specific surface area of the adsorbent.

3. Results and discussion

3.1. Preparation of CTF/Fe_2O_3 composites

We have recently demonstrated highly time- and energy-efficient synthesis of CTFs by using microwave-enhanced high-temperature ionothermal method, in which zinc chloride acts as a solvent of DCB, Lewis acid catalyst, as well as a microwave absorber. To obtain magnetic CTF composite containing ferric oxide particles, in the present work, a small amount of ferric chloride hexahydrate was introduced into the reaction mixture as a precursor of ferric oxide. Typical synthesis conditions, composition, porosity and magnetic properties of these CTF/Fe_2O_3 composites are summarized in Table 1.

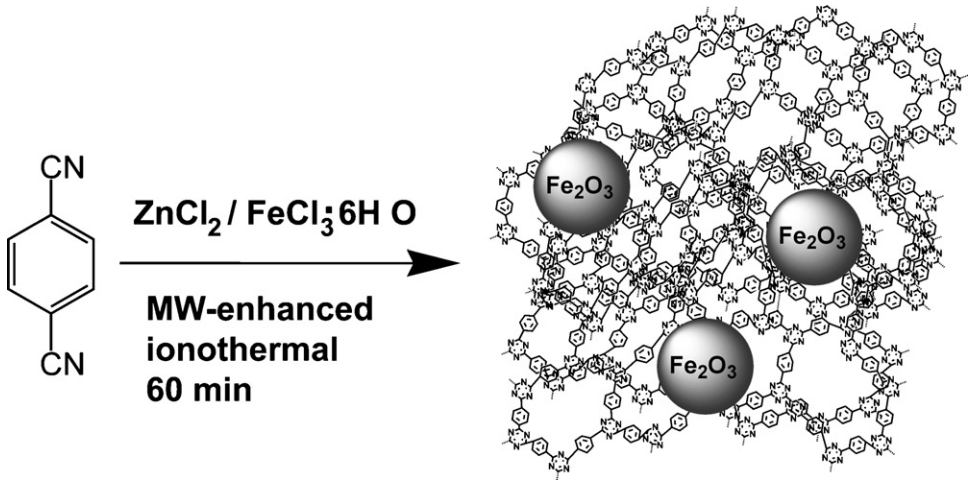

Fig. 1. Schematic illustration of CTF/Fe_2O_3 composite synthesized by the microwave-enhanced high-temperature ionothermal method.

Table 1
Synthetic parameters, porosity and magnetic properties of representative CTF/Fe_2O_3 composites.

Sample	$FeCl_3$/DCB weight ratio	Fe_2O_3 content (wt%)	Zn content (wt%)	C/N ratio	S_{BET} ($m^2\ g^{-1}$)	V_t ($cm^3\ g^{-1}$)	M_S (emu g^{-1})
1	3:100	6.43	10.50	9.555	1149	1.4	1.1
2	6:100	7.14	13.55	8.888	1080	1.5	3.1
3	9:100	7.64	13.06	9.859	930	1.3	3.3
4	12:100	11.14	6.15	9.228	1111	1.6	5.3
5	15:100	12.43	19.02	8.870	1092	1.6	5.9

All reactions were conducted in a high $ZnCl_2$/DCB ratio (5:1) in this work due to the fact that high $ZnCl_2$/DCB ratios always result in high performance CTFs [16–26]. Ionothermal polymerization of DCB catalyzed by $ZnCl_2$ in the presence of $FeCl_3$ at various $FeCl_3$/DCB weight ratios was carried out under microwave irradiation (350 W) for 1 h, resulting in a series of porous magnetic CTFs with different Fe_2O_3 contents. It was speculated that the excess of $ZnCl_2$ interacts strongly with the growing cyclic oligomers (through Lewis acid base interactions) [22]. To remove residual $ZnCl_2$, the products have to be washed using a large amount of water after the polymerization reaction. It was found that large amounts of $Zn(OH)_2$ precipitate were formed without the presence of HCl. This may lead to a significant decrease in surface area of the sample. Consequently, diluted HCl solution was used instead of water to avoid the hydrolysis of $ZnCl_2$ in aqueous solution. However, the composites still contain high amounts of residual zinc salts (Zn contents 6.15–19.02 wt%, see Table 1) that cannot be removed even after the samples were washed using a large amount of 0.1 M HCl. It should be noted, that $ZnCl_2$ can easily be removed after washing the samples with 1 M HCl solution, and contents of residual zinc salts in the final CTF products are commonly found to be lower than 5 wt% [16,20–22,25]. In this work, however, the CTF/Fe_2O_3 composites contain both residual zinc salts and iron oxide; washing the products using HCl with high concentrations led to remarkable decrease in iron oxide contents in the composites. As a result, 0.1 M HCl was used for the removal of zinc salts in this work.

3.2. Characterization of CTF/Fe_2O_3 composites

3.2.1. IR, XRD and XPS measurements

The polymerization of DCB was confirmed by FT-IR (see Fig. S1 in Supplementary Information). A strong band at 1515 cm^{-1} was observed and no carbonitrile band at 2236 cm^{-1} could be found from the FT-IR spectra, revealing the formation of triazine rings and a complete polymerization of DCB [16]. Structures of these CTF/Fe_2O_3 composites were also characterized by XRD (Fig. 2). Although crystalline CTF-1 samples containing hexagonal packing of micropores could be obtained by conventional ionothermal polymerization at a lower $ZnCl_2$/DCB ratio or at a lower reaction temperature, it was difficult to obtain crystalline CTF-type samples under such microwave-enhanced ionothermal conditions. A broad diffraction peak around $2\theta = 26.1^\circ$ was observed, and no peak could be found below 10°, revealing that amorphous CTF samples were obtained [20–22]. This is consistent with results obtained in our previous work, in which only amorphous CTF samples were obtained under such a microwave-enhanced high-temperature ionothermal condition [26]. Furthermore, elemental analyses of the samples reveal 2 times higher C/N ratio (8.870–9.859) of the samples synthesized under such microwave-enhanced conditions than that of an ideal CTF-1 structure. This could be attributed to the fast heating rate and high reaction temperature under microwave

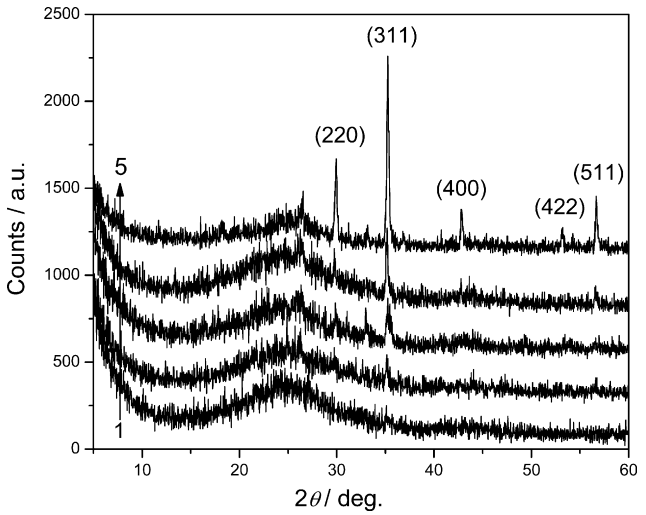

Fig. 2. XRD patterns of CTF/Fe_2O_3 composites containing different γ-Fe_2O_3 contents.

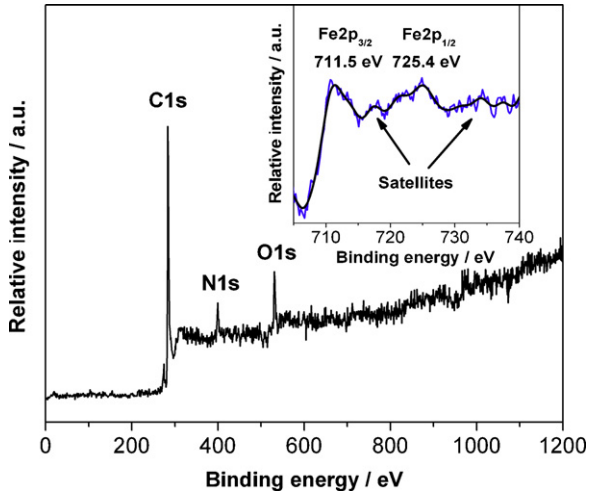

Fig. 3. XPS spectrum of CTF/Fe_2O_3 composite, showing the composition of γ-Fe_2O_3.

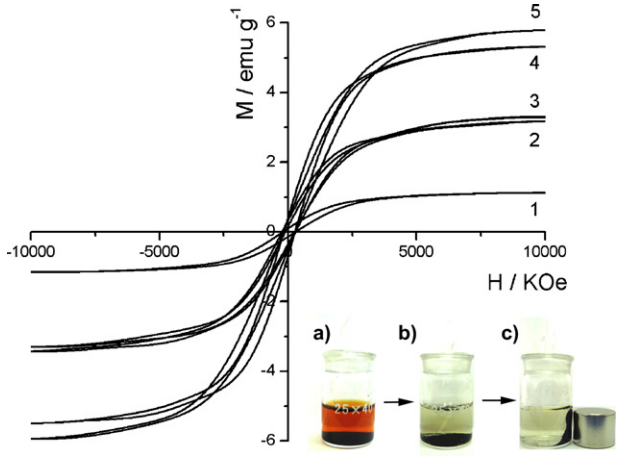

Fig. 4. Magnetization curves of CTF/Fe_2O_3 composites at 300 K; the inset shows methyl orange aqueous solution (a) before and (b) after the addition of CTF/Fe_2O_3 composite **4**, and (c) magnetic separation under an external magnetic field.

irradiation; in this case, C–C coupling reaction and further linkage of the aromatic building blocks via C–N eliminations occurs accompanying by the loss of nitrogen and hydrogen. In addition, a weak peak at 26.5° was found, which may be attributed to the formation of a small amount of graphitic carbon. Besides these two diffraction peaks, other peaks can be readily indexed to γ-Fe_2O_3 with the corresponding diffraction peaks of (2 2 0), (3 1 1), (4 0 0), (4 2 2), and (5 1 1) planes, respectively. Furthermore, with increasing γ-Fe_2O_3 content from 6.43 to 12.43 wt% in the composites (see Table 1), intensity of diffraction peaks corresponding to γ-Fe_2O_3 crystals increased gradually (Fig. 2).

In the case of small nanoparticles, it is difficult to distinguish between the γ-Fe_2O_3 and Fe_3O_4 phases based only on XRD analysis. To analyze composition of the sample, especially for clarifying the composition of magnetic particles in the composite, XPS measurements were conducted (Fig. 3). Three strong peaks located at 284.7, 400.3, and 531.8 eV are due to C 1s, N 1s, and O 1s binding energies for the composite, suggesting that the main content of the surface species is C, N, and O. Although XRD and atomic adsorption spectra results clearly revealed relatively high Fe_2O_3 contents (6.43–12.43 wt%) in the composites, the Fe 2p binding energies almost cannot be detected in wide-range XPS spectra of the sample. This is attributed to the fact that XPS analysis is a surface sensitive technique with a sampling volume that extends from the surface to a depth of 1–5 nm [27]. In the present work, magnetic γ-Fe_2O_3 nanoparticles in the composite are confined within pores in CTF matrix as clearly demonstrated by HRTEM image as shown below.

It is known that the presence of or the absence of charge transfer satellite near the photoelectron peak gives information about the oxidation of iron. The Fe $2p_{3/2}$ and $2p_{1/2}$ main peaks are always accompanied by satellites in a compound in which iron is the trivalent cationic form, while the charge transfer satellite disappears from the spectrum in mixed oxides of Fe^{2+} and Fe^{3+} [28]. To clarify the composition of the magnetic particles in the composites, high-resolution Fe 2p XPS spectrum was further measured (see inset in Fig. 3). Two peaks of bonding energies at 711.5 and 725.4 eV, corresponding to Fe $2p_{3/2}$ and Fe $2p_{1/2}$, respectively, were observed [28]. In addition, it can be clearly seen that satellites occur at 717.6 and 734.0 eV, respectively, which are characteristic for Fe^{3+} ions in Fe_2O_3 [28–30].

3.2.2. Magnetic properties

Fig. 4 shows the field-dependent magnetization curves of the CTF/Fe_2O_3 composites between ±10 kOe at 300 K. All magnetization curves exhibited a hysteresis loop, revealing ferromagnetic characteristic of the CTF/Fe_2O_3 composites. Saturation magnetizations (M_S) of these composites varied from 1.1 to 5.9 emu g^{-1}, depending on different Fe_2O_3 contents in the composites, suggesting that magnetic property of the composite can be tuned by controlling the synthesis parameters such as the ratio of Fe_2O_3 precursor (i.e. $FeCl_3$ in the present work) to 1,4-dicyanobenzene. It should be noted that, 2 mol of $FeCl_3{\cdot}6H_2O$ should result in 1 mol of Fe_2O_3 according to the formation mechanism. In principle, Fe_2O_3 content with an initial $FeCl_3$/DCB weight ratio of 3:100–15:100 would be approximately 1.5–7.5 wt%. However, Fe_2O_3 content in the composites varied from 6.43 to 12.43 wt%, which is much higher than the corresponding theoretical value. This can be attributed to low yields of CTF (25–60%) by using such microwave-assisted high-temperature ionothermal method because the polymerization reactions carried out at high-temperature under atmospheric pressure may lead to the oxidation and decomposition of monomer, oligomers, or the final products.

The adsorption ability and magnetic separability of the CTF/Fe_2O_3 composite were preliminarily tested by dispersing the

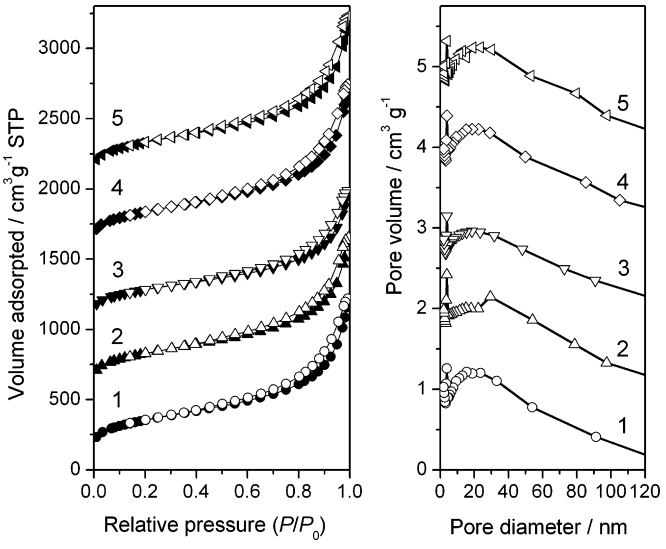

Fig. 5. N_2 sorption–desorption isotherms of CTF/Fe_2O_3 composites **1–5**, and pore diameter distributions. The isotherms for samples **2–5** were vertically offset by 500, 1000, 1500, and 2000 cm^3 g^{-1}, respectively. The distribution of pore diameters for samples **2–5** were vertically offset by 1, 2, 3, and 4 cm^3 g^{-1}, respectively.

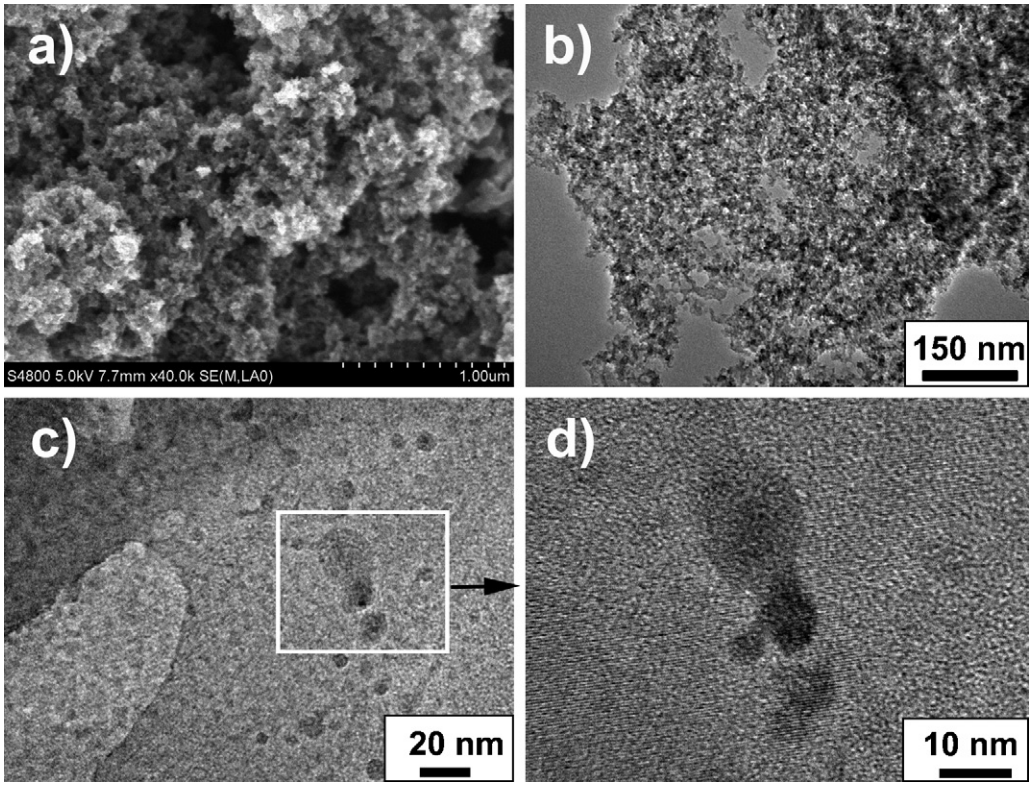

Fig. 6. Representative SEM (a) and TEM images (b–d) of the composites, revealing γ-Fe_2O_3 nanoparticles embedded in CTF support.

composite **4** in MO aqueous solution and shaking it for 30 min. After placing a magnet near the glass bottle, the black absorbent containing dye molecules were attracted to the magnet within few seconds (see the inset in Fig. 4). These results suggest that these CTF/Fe_2O_3 composites prepared are excellent candidates for magnetic separation of contaminants from aqueous solution.

3.2.3. N_2 sorption–desorption isotherms

The pore properties of the as-prepared CTF/Fe_2O_3 composites were investigated using N_2 sorption–desorption isotherms (see Fig. 5), and porosity properties of these composites are listed in Table 1. All samples exhibit a type IV isotherm, suggesting microporous materials with mesopores formed by close-packed nanoparticles. Pore size distribution analyses using the Barrett–Joyner–Halenda (BJH) method reveal a broad range of pore diameter distribution from 2 to 140 nm. The BET specific surface areas (S_{BET}) of the as-synthesized composites varied from 930 to 1149 $m^2\,g^{-1}$, and total pore volumes (V_t) of all samples are around 1.5 $cm^3\,g^{-1}$. These values surpass most of the magnetic carbon composites [11–15,31], as well as other magnetic composites such as mesoporous silica nanocomposite [32–34], as reported in the literature.

3.2.4. SEM and TEM investigations

Microstructures and porous characteristics of these CTF/Fe_2O_3 composites were investigated by SEM and TEM images. Fig. 6(a) and (b) shows the SEM and TEM images of a typical CTF/Fe_2O_3 composite. The porosity and texture of the sample are almost uniform as observed from both SEM and TEM images, and no obvious iron oxide particles with large size were detected, suggesting a complete inclusion of γ-Fe_2O_3 particles in the CTF/Fe_2O_3 composite. TEM results also clearly demonstrated that γ-Fe_2O_3 nanoparticles in a size range of 5–25 nm were well dispersed in the composite (see Fig. 6(c)–(d)). All these results reveal that γ-Fe_2O_3 nanocrystals are incorporated with amorphous CTF support, thus resulting in CTF/Fe_2O_3 composites.

3.3. Adsorption of methyl orange in CTF/Fe_2O_3 composite

3.3.1. Adsorption isotherms

Adsorption property of these CTF/Fe_2O_3 composites was demonstrated by using sample **4** as an absorbent and choosing MO as a model pollutant. Fig. 7 shows the adsorption isotherms of MO onto CTF/Fe_2O_3 composites. It can be seen that the adsorption capacities of MO increase sharply with an increase in MO equilibrium concentration when its value is lower than 12.5 $mg\,L^{-1}$. Above this concentration, however, increasing MO concentration does not affect adsorption capacity of MO, which is due to saturated adsorption of MO molecules onto the composite.

By fitting the equilibrium adsorption data with Langmuir adsorption model, adsorption capacity of MO onto the composite was calculated from Eq. (2) [14].

$$\frac{c_e}{q_e} = \frac{1}{bq_m} + \frac{c_e}{q_m} \quad (2)$$

where q_e ($mg\,m^{-2}$) is the equilibrium adsorption capacity, c_e ($mg\,L^{-1}$) is the equilibrium concentration of dye in the solution, q_m ($mg\,m^{-2}$) is the monolayer adsorption capacity, and b ($L\,mg^{-1}$) is the Langmuir constant.

The linear regression between c_e/q_e and c_e was calculated, and the correlation coefficient of the straight line is 0.9842, indicating that the adsorption of MO conforms Langmuir's adsorption model. Significantly, adsorption capacity of MO onto sample **4** was calculated to be 291 $mg\,g^{-1}$ (corresponding to 0.889 $mmol\,g^{-1}$ or 0.262 $mg\,m^{-2}$), which is much larger than that of many other magnetic porous composites [7–15]. Interestingly, this value is even larger than MO adsorption amounts in porous chromium-benzenedicarboxylates (MIL-101, ethylenediamine-grafted MIL-101, and the protonated ED-MIL-

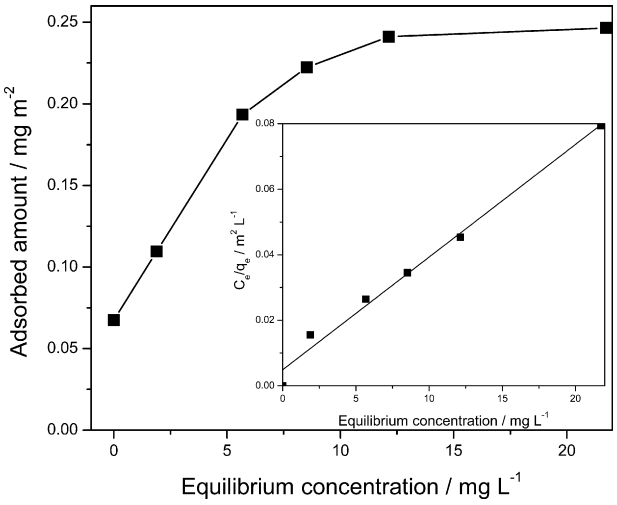

Fig. 7. Adsorption isotherms of methyl orange onto CTF/Fe_2O_3 composite **4**, and the linear regression by fitting the equilibrium adsorption data with Langmuir adsorption model.

101), a series of metal-organic frameworks (MOFs) with ultrahigh surface area (S_{BET} = 3296–3873 $m^2\ g^{-1}$) [36].

3.3.2. Adsorption kinetics

To have a better understanding of adsorption kinetics, the effect of contact time on the adsorption of MO onto CTF/Fe_2O_3 composite was investigated by adding 25 mg of **4** to 50 mL of 50 mg L^{-1} MO solution. As can be seen in Fig. 8, the sample attained over 90% of the adsorption capacity at equilibrium within 30 min, suggesting that the magnetic composite possesses both a high adsorption capacity and a high adsorption efficiency for the removal of pollutants from water. This could be attributed to a broad pore diameter distribution from micropore to mesopore of the sample (Fig. 5), because adsorption kinetics of materials with such a broad pore diameter distribution is quite similar to that of hierarchically micro- and mesoporous materials.

The kinetics parameters were analyzed by the pseudo-second-order kinetic equation [11,14,35]:

$$\frac{t}{q_t} = \frac{1}{k_2 q_e^2} + \frac{t}{q_e} \quad (3)$$

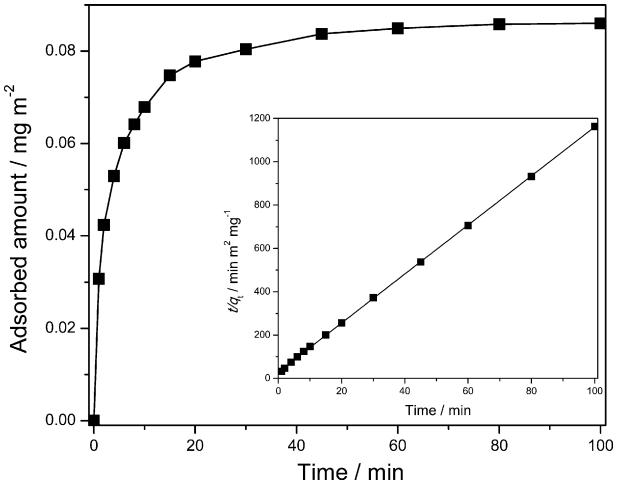

Fig. 8. Adsorption curve of methyl orange by CTF/Fe_2O_3 composite **4** versus contact time in aqueous solution, and the pseudo-second-order kinetic plot for the adsorption (MO concentration: 50 mg L^{-1}).

where k_2 ($m^2\ mg^{-1}\ min^{-1}$) is the pseudo-second-order adsorption rate constant.

By fitting the experimental data with the pseudo-second-order kinetic model using Eq. (3), the pseudo-second-order adsorption rate constant k_2 was obtained. The correlation coefficient for the fitting is 0.9998, suggesting the adsorption of MO onto surface of the adsorbent follows a pseudo-second-order kinetic model. Value of k_2 under this condition in the present work was determined to be 4.31 $m^2\ mg^{-1}\ min^{-1}$ (corresponding to 3.88×10^{-3} g $mg^{-1}\ min^{-1}$). This value also exceeds many magnetic absorbents including some hierarchically porous materials [11,37–39], which can also be attributed to large pore volumes (1.3–1.6 $cm^3\ g^{-1}$) of amorphous CTF materials and a broad pore distribution from microporous to mesoporous regimes in the solids as mentioned above [20–22,26].

4. Conclusions

We have demonstrated a facile method for the rapid synthesis of magnetic carbonaceous polymer composites with both high adsorption capacity and magnetic characteristic, as well as rapid adsorption kinetics, for the removal of dye from aqueous solution. A novel kind of covalent triazine-based framework-Fe_2O_3 composite was prepared by a microwave-enhanced high-temperature ionothermal method. The magnetic composites exhibit both high BET surface areas (930–1149 $m^2\ g^{-1}$) and total pore volumes (1.3–1.6 $cm^3\ g^{-1}$). It was found that magnetic property of the composites could be tuned by varying weight ratio of 1,4-dicyanobenzene to $FeCl_3$. The magnetic separation of pollutants was investigated preliminarily by choosing methyl orange as a model pollutant. Both high adsorption capacity (291 mg g^{-1}) and fast adsorption kinetics (k_2 = 4.31 $m^2\ mg^{-1}\ min^{-1}$) were obtained for the removal of methyl orange from aqueous solution. We believe the results presented here open a new opportunity for the large-scale industrial preparation of magnetic carbonaceous absorbents and their application in magnetic separation of contaminants from aqueous solution.

Acknowledgments

This work was supported by the National Natural Science Foundation of China (20971001), the NSFC-CAS Joint Fund for Research Based on Large-Scale Scientific Facilities (10979014), the Program for New Century Excellent Talent in University, Ministry of Education, China (NCET-08-0617), the "Hundred Talents Program" of the Chinese Academy of Sciences, the Natural Science Foundation of Anhui Province, China (Grant 090414164), and the "211 Project" of Anhui University.

Appendix A. Supplementary data

Supplementary data associated with this article can be found, in the online version, at doi:10.1016/j.jhazmat.2010.11.093.

References

[1] A.R. Cestari, E.F.S. Vieira, A.A. Pinto, E.C.N. Lopes, Multistep adsorption of anionic dyes on silica/chitosan hybrid. 1. Comparative kinetic data from liquid- and solid-phase models, J. Colloid. Interface Sci. 292 (2005) 363–372.
[2] Y.C. Wong, Y.S. Szeto, W.H. Cheung, G. Mckay, Pseudo-first-order kinetic studies of the sorption of acid dyes onto chitosan, J. Appl. Polym. Sci. 92 (2004) 1633–1645.
[3] G. Crini, Non-conventional low-cost adsorbents for dye removal: a review, Bioresour. Technol. 97 (2006) 1061–1085.
[4] N. Graham, X.G. Chen, S. Jeyaseelan, The potential application of activated carbon from sewage sludge to organic dyes removal, Water Sci. Technol. 34 (2001) 245–252.
[5] M.J. Martin, A. Artola, B.M. Dolors, M. Rigola, Activated carbons developed from surplus sewage sludge for the removal of dyes from dilute aqueous solutions, Chem. Eng. J. 94 (2003) 231–239.

[6] D. Clifford, P. Chu, A. Lau, Thermal regeneration of powdered activated carbon (PAC) and PAC-biological sludge mixtures, Water Res. 17 (1983) 1125–1138.
[7] A. Afkhami, R. Moosavi, Adsorptive removal of Congo red, a carcinogenic textile dye, from aqueous solutions by maghemite nanoparticles, J. Hazard. Mater. 174 (2010) 398–403.
[8] S. Qadri, A. Ganoe, Y. Haik, Removal and recovery of acridine orange from solutions by use of magnetic nanoparticles, J. Hazard. Mater. 169 (2009) 318–323.
[9] L. Zhou, C. Gao, W. Xu, Magnetic dendritic materials for highly efficient adsorption of dyes and drugs, ACS Appl. Mater. Interface 2 (2010) 1483–1491.
[10] S.Y. Mak, D.H. Chen, Fast adsorption of methylene blue on polyacrylic acid-bound iron oxide magnetic nanoparticles, Dyes Pigments 61 (2004) 93–98.
[11] D.W. Wang, F. Li, G.Q. Lu, H.M. Cheng, Synthesis and dye separation performance of ferromagnetic hierarchical porous carbon, Carbon 46 (2008) 1593–1599.
[12] N. Yang, S. Zhu, D. Zhang, S. Xu, Synthesis and properties of magnetic Fe_3O_4-activated carbon nanocomposite particles for dye removal, Mater. Lett. 62 (2008) 645–647.
[13] L.C.A. Oliveira, R.V.R.A. Rios, J.D. Fabris, V. Garg, K. Sapag, R.M. Lago, Activated carbon/iron oxide magnetic composites for the adsorption of contaminants in water, Carbon 40 (2002) 2177–2183.
[14] L. Ai, H. Huang, Z. Chen, X. Wei, J. Jiang, Activated carbon/$CoFe_2O_4$ composites: facile synthesis, magnetic performance and their potential application for the removal of malachite green from water, Chem. Eng. J. 156 (2010) 243–249.
[15] S. Qu, F. Huang, S. Yu, G. Chen, J. Kong, Magnetic removal of dyes from aqueous solution using multi-walled carbon nanotubes filled with Fe_2O_3 particles, J. Hazard. Mater. 160 (2008) 643–647.
[16] P. Kuhn, M. Antonietti, A. Thomas, Porous, covalent triazine-based framework prepared by ionothermal synthesis, Angew. Chem. Int. Ed. 47 (2008) 3450–3453.
[17] A.P. Côté, A.I. Benin, N.W. Ockwing, M. O'Keeffe, A.J. Matzger, O.M. Yaghi, Porous, crystalline, covalent organic frameworks, Science 310 (2005) 1166–1170.
[18] M. Mastalerz, The next generation of shape-persistent zeolite analogues-covalent organic frameworks, Angew. Chem. Int. Ed. 47 (2008) 445–447.
[19] K.E. Maly, Assembly of nanoporous organic materials from molecular building blocks, J. Mater. Chem. 19 (2009) 1781–1787.
[20] P. Kuhn, A. Forget, D. Su, A. Thomas, M. Antonietti, From microporous regular frameworks to mesoporous materials with ultrahigh surface area: dynamic reorganization of porous polymer networks, J. Am. Chem. Soc. 130 (2008) 13333–13337.
[21] P. Kuhn, A. Forget, J. Hartmann, A. Thomas, M. Antonietti, Template-free tuning of nanoporous in carbonaceous polymers through ionothermal synthesis, Adv. Mater. 21 (2009) 897–901.
[22] P. Kuhn, A. Thomas, M. Antonietti, Toward tailorable porous organic polymer networks: a high-temperature dynamic polymerization scheme based on aromatic nitriles, Macromolecules 42 (2009) 319–326.
[23] R. Palkovits, M. Antonietti, P. Kuhn, A. Thomas, F. Schüth, Solid catalysts for the selective low-temperature oxidation of methane to methanol, Angew. Chem. Int. Ed. 48 (2009) 6909–6912.
[24] C.E. Chan-Thaw, A. Villa, P. Katekomol, D. Su, A. Thomas, L. Prati, Covalent triazine framework as catalytic support for liquid phase reaction, Nano Lett. 10 (2010) 537–541.
[25] P. Kuhn, K. Krüger, A. Thomas, M. Antonietti, Everything is surface: tunable polymer organic frameworks with ultrahigh dye sorption capacity, Chem. Commun. (2008) 5815–5817.
[26] W. Zhang, C. Li, Y.P. Yuan, L.G. Qiu, A.J. Xie, Y.H. Shen, J.-F. Zhu, Highly energy- and time-efficient synthesis of porous triazine-based framework: microwave-enhanced ionothermal polymerization and hydrogen uptake, J. Mater. Chem. 20 (2010) 6413–6415.
[27] Ş. Süzer, XPS investigation of X-ray-induced reduction of metal ions, Appl. Spectrosc. 54 (2000) 1716–1718.
[28] M. Descostes, F. Mercier, N. Thromat, C. Beaucaire, M. Gautier-Soyer, Use of XPS in the determination of chemical environment and oxidation state of iron and sulfur samples: constitution of a data basis in binding energies for Fe and S reference compounds and applications to the evidence of surface species of an oxidized pyrite in a carbonate medium, Appl. Surf. Sci. 165 (2000) 288–302.
[29] T. Fujii, F.M.F. de Groot, G.A. Sawatzky, F.C. Voogt, T. Hibma, K. Okada, In situ XPS analysis of various iron oxide films grown by NO_2-assisted molecular-beam epitaxy, Phys. Rev. B 59 (1999) 3195–3202.
[30] C. Pascal, J.L. Pascal, F. Favier, Electrochemical synthesis for the control of γ-Fe_2O_3 nanoparticle size, morphology, microstructure, and magnetic behavior, Chem. Mater. 11 (1999) 141–147.
[31] J. Lee, S. Jin, Y. Hwang, J.G. Park, H.M. Park, T. Hyeon, Simple synthesis of mesoporous carbon with magnetic nanoparticles embedded in carbon rods, Carbon 43 (2005) 2536–2543.
[32] T. Sen, A. Sebastianelli, I.J. Bruce, Mesoporous silica magnetite nanocomposite: fabrication and applications in magnetic bioseparations, J. Am. Chem. Soc. 128 (2006) 7130–7131.
[33] J. Kim, J.E. Lee, J. Lee, J.H. Yu, B.C. Kim, K. An, et al., Magnetic fluorescent delivery vehicle using uniform mesoporous silica spheres embedded with monodisperse magnetic and semiconductor nanocrystals, J. Am. Chem. Soc. 128 (2006) 688–689.
[34] W. Zhao, J. Gu, L. Zhang, H. Chen, J. Shi, Fabrication of uniform magnetic nanocomposite spheres with a magnetic core/mesoporous silica shell structure, J. Am. Chem. Soc. 127 (2005) 8916–8917.
[35] Y.S. Ho, G. McKay, Sorption of dye from aqueous solution by peat, Chem. Eng. J. 70 (1998) 115–124.
[36] E. Haque, J.E. Lee, I.T. Jang, Y.K. Hwang, J.-S. Chang, J. Jegal, S.H. Jhung, Adsorptive removal of methyl orange from aqueous solution with metal-organic frameworks, porous chromium-benzenedicarboxylates, J. Hazard. Mater. 181 (2010) 535–542.
[37] Z.H. Sun, L.F. Wang, P.P. Liu, S.C. Wang, B. Sun, D.Z. Jiang, et al., Magnetically motive porous sphere composite and its excellent properties for the removal of pollutants in water by adsorption and desorption cycles, Adv. Mater. 18 (2006) 1968–1971.
[38] S. Chen, J. Zhang, C. Zhang, Q. Yue, Y. Li, C. Li, Equilibrium and kinetic studies of methyl orange and methyl violet adsorption on activated carbon derived from Phragmites australis, Desalination 252 (2010) 149–156.
[39] H.Y. Zhu, R. Jiang, L. Xiao, G.M. Zeng, Preparation, characterization, adsorption kinetics and thermodynamics of novel magnetic chitosan enwrapping nanosized γ-Fe_2O_3 and multi-walled carbon nanotubes with enhanced adsorption properties for methyl orange, Bioresour. Technol. 101 (2010) 5063–5069.